Medical Engineering and Physics 38 (2016) 538–546

Contents lists available at ScienceDirect

Medical Engineering and Physics

journal homepage: www.elsevier.com/locate/medengphy

A method to adapt thoracic impedance based on chest geometry and composition to assess congestion in heart failure patients

Illapha Cuba-Gyllensten[a,b,*], Paloma Gastelurrutia[c], Alberto G. Bonomi[a], Jarno Riistama[a], Antoni Bayes-Genis[c,d], Ronald M. Aarts[a,b]

[a] Department of Chronic Disease Management, Philips Research, Eindhoven, the Netherlands
[b] Department of Electrical Engineering, Eindhoven University of Technology, Eindhoven, the Netherlands
[c] ICREC Research Program, Fundació Institut d'Investigació en Ciències de la Salut Germans Trias i Pujol (IGTP), Badalona, Spain
[d] Department of Medicine, Universitat Autònoma de Barcelona, Barcelona, Spain

ARTICLE INFO

Article history:
Received 13 May 2015
Revised 18 January 2016
Accepted 6 March 2016

Keywords:
Heart failure
Bioimpedance spectroscopy
Personalization
Simulation
Decompensation

ABSTRACT

Multi-frequency trans-thoracic bioimpedance (TTI) could be used to track fluid changes and congestion of the lungs, however, patient specific characteristics may impact the measurements. We investigated the effects of thoracic geometry and composition on measurements of TTI and developed an equation to calculate a personalized fluid index. Simulations of TTI measurements for varying levels of chest circumference, fat and muscle proportion were used to derive parameters for a model predicting expected values of TTI. This model was then adapted to measurements from a control group of 36 healthy volunteers to predict TTI and lung fluids (fluid index). Twenty heart failure (HF) patients treated for acute HF were then used to compare the changes in the personalized fluid index to symptoms of HF and predicted TTI to measurements at hospital discharge. All the derived body characteristics affected the TTI measurements in healthy volunteers and together the model predicted the measured TTI with 8.9% mean absolute error. In HF patients the estimated TTI correlated well with the discharged TTI ($r = 0.73$, $p < 0.001$) and the personalized fluid index followed changes in symptom levels during treatment. However, 37% ($n = 7$) of the patients were discharged well below the model expected value. Accounting for chest geometry and composition might help in interpreting TTI measurements.

1. Introduction

Congestion is a defining feature of decompensated heart failure (HF), a frequent cause for hospitalization, and a main target during treatment [1]. Despite this, there is a paucity of tools that provide a quantified assessment of the level of congestion. Current tools are often complex requiring invasive measurements to establish heamodynamic pressures or chest x-rays which exposes the patient to ionizing radiation and give equivocal results. Clinical judgment on the other hand is often inexact and requires substantial clinical acumen [2]. Preferably methods that establish congestion should be simple and easy to use with reliable results.

Trans-thoracic bioimpedance (TTI) can be used to assess tissue hydration as increased fluid levels increase the conductivity of the tissue. This has been used to show that non-invasive measurements of impedance at a single frequency correlates with radiographic and clinical indices of pulmonary oedema in HF patients [3,4]. Different frequencies have different progressions [5] and multi-frequency measurements can be used to improve estimates of body fluids by modeling the spectroscopic response [6]. For living biological tissues measured in the kilohertz to megahertz range this response, β dispersion, can be approximated by a Cole model [7]. This empirical model describes the impedance based on four variables: R_0, the extrapolated zero frequency or DC component; R_∞, the extrapolated infinite frequency component; f_C, the characteristic frequency; and α, the dispersion parameter [8]. At low frequencies the resistance is impacted by the extra-cellular fluids to a larger extent than at higher frequencies, for which a larger part of the current passes through the cell membranes. Increased fluids in the lung interstitium and later into the alveoli should thus be reflected in the DC component of the model, R_0.

A challenge with bioimpedance measures is that the individual optimal value depends on the morphology and distribution of the different tissues. Without a target value one can only establish relative changes in fluid levels which can be difficult to interpret and

* Corresponding author at: Department of Personal Health Solutions, Philips Research, Eindhoven, the Netherlands. Tel.: +31 631 926 930.
E-mail address: illapha@gmail.com (I. Cuba-Gyllensten).

http://dx.doi.org/10.1016/j.medengphy.2016.03.002
1350-4533/

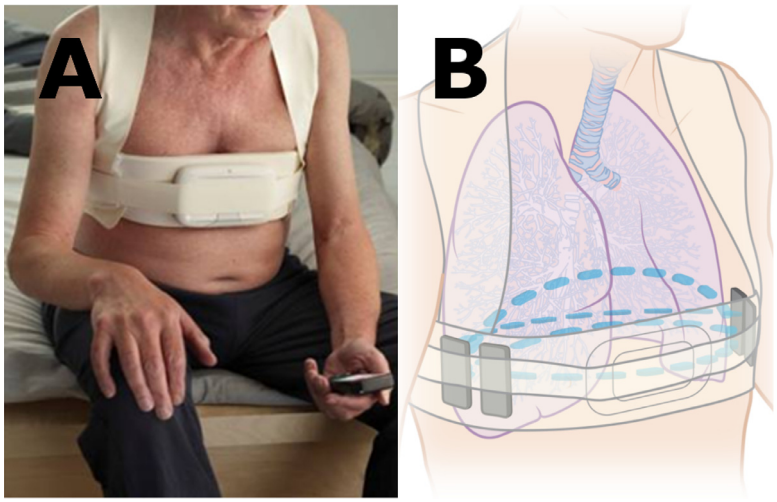

Fig. 1. The portable measurement device and vest. A: actual device showing proper placement (person shown is not a participant in the trials but a model) B: transparent sketch of the device showing the four textile electrodes and lungs [48].

use for clinical decisions. Multiple meticulously placed electrodes could be added measuring impedance between different configurations [9]. The resulting data could then be used to compute the likely contribution of different regions to the total impedance which addresses this shortcoming to a certain extent, but which might be difficult to apply in practice. Other frequency ranges that have been explored to establish lung fluid content from changed dielectric properties include RF [10] and microwave reflectometry [11]. Ideally, the system should be easy enough for daily monitoring, preferably applied by the patients themselves.

The aim of this study was to investigate a normalization method for a tetrapolar setup of trans-thoracic bioimpedance (TTI) measurement integrated into a wearable system. First, the relationships between TTI, the geometry, and the thoracic tissue composition (fat, muscle, and dry or fluid filled lungs) were explored using a simulation model (Sections 3.1 and 3.2). Results from the simulation model were then adapted to receive as input simple anthropomorphic measures to model TTI measurements from healthy "control" subjects (Section 4.1). Measurements from HF patients discharged after an episode of acute decompensation were then compared to the expected values from this TTI estimation model (Section 4.2). Finally, changes in an index based on the model and the estimated change in response to fluids (Section 3.2) was derived for the HF patients during a series of measurements from admission of acute decompensation up until hospital discharge and compared to assessments of symptoms of congestion (Section 4.3).

2. Materials and methods

2.1. The measurement vest

The wearable system was developed to provide an easy and simple method to reliably measure TTI so that it could be done by patients on their own. The system can connect to a mobile phone or tablet making it possible to guide the patient through the measurement and thus ensure proper posture and reduce inadvertent movements during a measurement.

The system is shown in Fig. 1 together with a schematic of the setup. It consists of three parts: an adjustable vest, a measurement device and a rigid panel with electrodes. The four textile electrodes on the panel are made of silver coated polyurethane yarn for comfort and kept at proper distance by the panel. The panel is wrapped around the chest at, approximately, the level of the tenth rib and kept together with the adjustable vest. The measurement device is then connected to the setup to inject current and log the resulting voltages (Philips Technologie Gmbh, Aachen, Germany) [12]. Sixteen frequencies are measured sequentially (10 kHz–1 MHz) during one acquisition. Before any measurements the textile electrodes are wetted to lower the interface impedance to the skin.

2.2. Simulation of thorax

A finite element method simulation of the setup was carried out to evaluate the theoretical influence of chest geometry and composition on the spectroscopic measurements. This approach has previously been applied to determine effects of thoracic fluids on impedance cardiography [13] and electrode placement [14,15]. To easily scale the different compositions of fat, muscle and circumference a simplified model of the human thorax was constructed based on the tissue proportions just above the liver from a computer tomography scan. The complex ovaloid shape was approximated as a series of concentric circles surrounding the lungs which simplifies scaling, see Fig. 2. Simple structures of ribs, spines, heart, and liver was added to the model in proportion with the tissues of the scan (See supplemental file for the geometric equations).

Dielectric properties of the tissues were taken from the equations provided by Gabriel [16]. The constants for deflated lung, infiltrated fat, transverse muscle, blood, cortical bone, heart, liver, and dry skin were used for the tissues representing lung, fat, muscle, fluids, bone, liver, and skin respectively. Fig. 3 shows the permittivity and conductivity of the first four of these parameters between 10 kHz and 1 MHz. Meshes were created for chest circumferences from 80 to 120 cm in increments of 10 cm in chest circumference. Fat layer and muscle layer were varied in proportion to the chest radius. Added muscle in proportion to chest radius was varied between 0 and 8% in increments of 2% and fat layer was varied between 3% and 15% in increments of 3%. For each mesh transfer impedances were calculated for 16 logarithmically spaced frequencies between 10 kHz and 1 MHz. All simulations were carried out in COMSOL 4.4 [17].

2.3. Data and study protocols

Real measurement data for model development and evaluation was taken from two trials. One on healthy subjects (control subjects) enrolled in a body-composition trial and a second one on

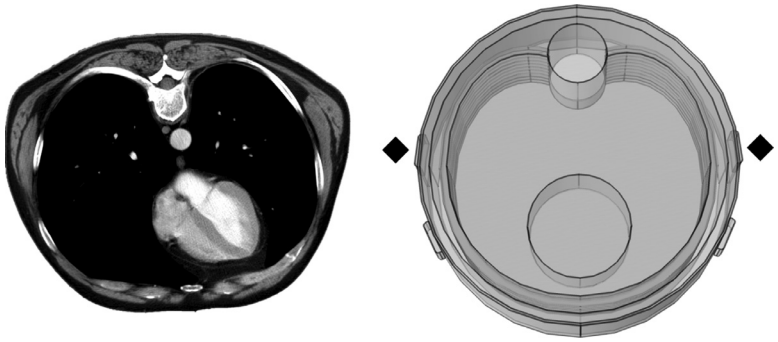

Fig. 2. Axial reconstruction of a thoracic CT-scan just above the liver and the simplified circular 3D model used for simulating transfer impedances. The two current carrying electrodes are marked with a rhombus. The voltage electrodes are visible underneath.

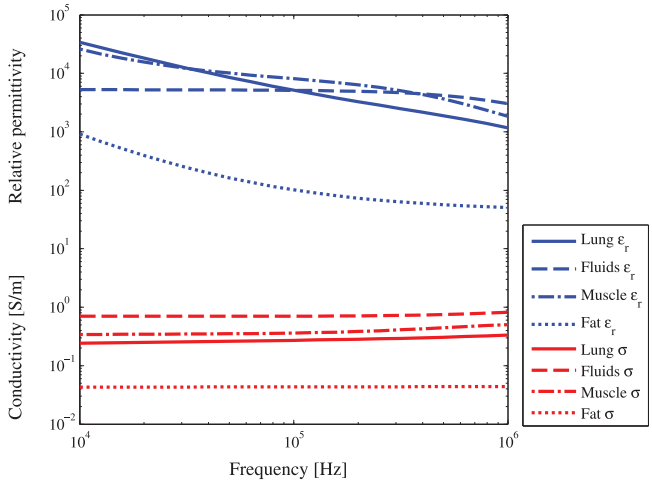

Fig. 3. Permittivity and conductivity given by the equations provided by Gabriel et al. in the range from 10 kHz to 1 MHz. At 10 kHz the corresponding resistivity of the conductivity values are 412, 143, 293, and 2326 Ω · cm for lung, fluid, muscle and fat tissue, respectively.

HF patients receiving treatment for acute decompensated HF. Both study protocols were subjected to review by an ethical committee (separate for each study) and approved. Informed consent was sought and obtained for all the participants in the trials. Details of each trial are described in the following subsections.

2.3.1. Control subjects with normal lung fluids

Subjects in the trial were enrolled for a day of measurements during which the following methods of body-composition were assessed: under water weighing, deuterium solution, subcutaneous fat estimates from ultra sound, and caliper measurements of skin folds. On the intake day prior to any tests each subject in the trial was properly informed and provided informed consent. Subjects were then asked to report back the following morning on an empty stomach between 8:00 and 10:00 for TTI measurements and body-composition assessment.

In total 49 subjects were enrolled out of which 36 subjects had analyzable measurements of bioimpedance and the necessary body composition parameters.

2.3.2. Subjects hospitalized for acute heart failure

The study and protocol has been described previously [18] where the vests ability to track fluid loss (weight), its relationship with improvements in symptoms, and NT-proBNP[1] was assessed. Patients who were admitted to the cardiology ward for acute decompensated HF and provided informed consent were included if none of the exclusion criteria were met, detailed in supplementary files. Skinfold measurements and chest circumference were made on the inclusion day. TTI measurements, taken in a semi-recumbent position with the ward couch lifted to 30 degrees, were made on the inclusion day, on the three subsequent days, and at discharge, together with a clinician-assessed heart failure severity score (HFSS). Based on the Framingham criteria [19] the HFSS provides a quantified score of the symptom level and was used to assess severity of heart failure decompensation and congestion from fluid accumulation. Major criteria (paroxysmal nocturnal dyspnea, basal crackles, positive hepatojugular reflex, and third heart sound) were assigned values of 1, and minor criteria (orthopnea, reduction in exercise tolerance, resting sinus tachycardia, jugular venous pressure >4 cm, hepatomegaly, and peripheral edema) were assigned values of 0.5 with the total sum representing the clinical congestion status [20,21].

In total 22 subjects were enrolled of which two were excluded from the analysis due to deviating morphology hindering proper vest use. One patient lacked a recording of discharge weight and was therefore not used for fluid index calculation. The general characteristics of the subjects are shown in Table 1, the clinical characteristics of the HF patients are provided in the supplemental files.

Table 1
Subject characteristics (mean and standard deviation).

	Control subjects ($n = 36$)	Heart failure patients ($n = 20$)
Sex	50% male ($n = 18$)	85% male ($n = 17$)
Age	29.8 ± 11.3 years	74.7 ± 9.5 years
Height	174 ± 7.5 cm	166 ± 9.2 cm
BMI	23.2 ± 2.6 kg/m^2	25.8 ± 4.4 kg/m^2
Bodyfat	23.4 ± 9.5%	27.2 ± 6.4%
Chest circumference	81.8 ± 8.2 cm	100.0 ± 9.2 cm
Subscapular skinfold	12.9 ± 4.0 mm	18.3 ± 5.8 mm
FFMi	17.4 ± 2.1 kg/m^2	18.7 ± 2.8 kg/m^2

2.4. Cole model fitting

The Cole model (see Eq. (1)) was fitted to the measurements from the device, or in the case of the simulations to the simulated transfer impedances, by non-linear minimization of the root mean-squared error of the conductance [22]. The R_0 parameter of the Cole model is thought to primarily reflect extracellular fluids thus this was used to characterize the thorax. For simplicity we will use "impedance" when discussing our results in the text to refer to the value of the fitted R_0 parameter of the Cole-model (unless a

[1] A common prognostic biomarker for HF.

specific frequency is noted).

$$Z = R_\infty + \frac{R_0 - R_\infty}{1 + (jw\tau)^\alpha}. \quad (1)$$

2.5. Development of R_0 prediction from morphology

The data from the 125 simulations with differing geometries and compositions were imported into Matlab (R2014a) and the Cole model parameter R_0 was fitted. The values were then explored to establish three calculated variables from circumference (l_{circ}), fat proportion (p_{fat}), and muscle (p_{muscle}) that affected measured impedance in an independent manner.

Following the identification of the relationships linking the three variables (l_{circ}, p_{fat}, and p_{muscle}) to R_0, these where extracted from actual subjects according to measurements of chest circumference and skin caliper measurements. Chest circumference was used as a surrogate for l_{circ} and thoracic fat proportion was then calculated based on the subscapular skin caliper measurement:

$$\hat{p}_{fat} = \frac{\pi \cdot Skinfold_{subscapular}}{\hat{l}_{circ}}. \quad (2)$$

Ultrasound could be used to provide a measure of localized skeletal muscle, however this information was not recorded for the subjects in the trials. Fat free mass is a simpler measure to estimate and its major component is muscle. This could then be used as a surrogate measure. However, as a percentage value it is unsatisfactory since it depends on height [23,24]. Fat free mass index (FFMi) on the other hand is independent of height [25] and relates to the total proportion of height adjusted fat free mass. This provided a pragmatic solution to the parameter representing muscle proportion, although a global and not a local measure. To establish the FFMi the fatmass percentage was estimated based on the skinfold measurements, age, and sex using the tables provided by Durnin and Womersley [26] and then height normalized:

$$p_{muscle} \propto \frac{Weight \cdot (100 - Fatmass\%)}{Height^2}. \quad (3)$$

These translated values were then used to construct a model of dry thoracic impedance (i.e. thoracic impedance without any congestion) based on the control subjects by means of linear least squares fitting to the observed R_0 values.

2.6. Fluid index model

To establish the estimated fluid index the measured R_0 was compared to the model expected dry thoracic impedance $\hat{R}_0$ and the expected impedance with fluid filled lungs. This was established by multiplying the model expected dry impedance with the percentage drop in impedance p_{fluids} established from finite element simulations replacing the dielectric properties of the lung tissue with fluids. A fluid index of 0 corresponds to a measured R_0 equal to the model expected value and 1 to a measured R_0 equal to the model expected value for fully fluid filled lungs. Effects of fluid accumulation in other tissues was omitted from this model.

$$\text{fluid index} = \frac{\hat{R}_0 - R_0}{\hat{R}_0 - \hat{R}_0 \cdot p_{fluids}}. \quad (4)$$

2.7. Statistics and model evaluation

Fitted impedance estimates $\hat{R}_0$ to observed R_0 were evaluated using Pearson product-moment correlation coefficients (r), root mean squared errors (RMSE), and mean absolute errors (MAE), reported unadjusted. Relationships between the aggregated heart failure severity score (HFSS) derived from symptoms and the calculated fluid index during treatment for acute heart failure was analyzed with a linear mixed effect model. Individual symptoms were analyzed with both uni- and multi-variate linear mixed effect models. As fixed effects, we entered the HFSS or the individual symptom. As random effects, we used patient specific intercepts. All models were fitted using maximum likelihood estimation by a quasi-newton optimizer. A nominal significance level of 0.05 was assumed throughout. All statistical and evaluation metrics were developed in a Matlab (R2014a) environment.

3. Simulation results

3.1. Morphology dependencies from simulation

Impedance variation as a function of chest circumference and muscle proportion, see Fig. 4, was found to be approximately linear with the chord length between the electrodes i.e. the straight distance between the electrodes. Expressing the chord length as a function of the electrode panel length and chest circumference gives the following equation:

$$l_{chord} = \frac{l_{circ}}{\pi} \cdot \sin\left(\frac{\pi \cdot l_{panel}}{l_{circ}}\right), \quad (5)$$

where l_{chord} is the chord distance, l_{circ} is the circumference, and l_{panel} the length of the panel between the electrodes. The chord length is then simply multiplied with the proportion of muscle (p_{muscle}) to give l_{muscle}:

$$l_{muscle} = p_{muscle} \cdot l_{chord}. \quad (6)$$

Increased fat, being more resistive than the other tissues, had a greater impact the larger the proportion was, see Fig. 4. In the explored ranges it could be approximated by the volume of fat multiplied by the squared proportion of fat or k_{fat}. Since the height of the electrodes is constant the fat volume is proportional to the hollow circle area:

$$A_{fat} = (2p_{fat} - p_{fat}^2) \cdot \frac{l_{circ}^2}{4\pi} \quad (7)$$

$$k_{fat} = A_{fat} \cdot p_{fat}^2. \quad (8)$$

Where p_{fat} is the proportion of the radius that is fat. A more detailed derivation of the geometric relationships can be found in the supplemental files. The three calculated variables (l_{chord}, l_{muscle} and k_{fat}) were then combined into a linear model to predict the expected impedance with coefficients x_1, x_2, and x_3, and a constant term x_4:

$$\hat{R}_0 = x_1 \cdot l_{chord} + x_2 \cdot l_{muscle} + x_3 \cdot k_{fat} + x_4. \quad (9)$$

The simulation generated transfer impedances which were more complex than what could be captured by this descriptive linear expression. To improve slightly on this one could account for the angle between the electrodes and the circle center. A smaller angle would mean that there will be more heart and muscle tissues between the electrodes and thus influence the result.

$$\theta = 2\pi \cdot \frac{l_{panel}}{l_{circ}}, \quad (10)$$

$$\hat{R}_0 = x_1 \cdot l_{chord} + x_2 \cdot l_{muscle} + x_3 \cdot k_{fat} + x_4 \cdot \theta + x_5. \quad (11)$$

The RMSE between the 125 simulation results and the linear expression was 0.297 Ω, or 0.325 Ω omitting the angle contribution, providing adequate accuracy for chest, fat, and muscle distributions in this physiological range. The coefficients for the two fittings were: $x_1 = -409$, $x_2 = -241$, $x_3 = 0.78 \cdot 10^4$, $x_4 = 11$, and $x_5 = -87$ (Eq. (11)); and $x_1 = 162$, $x_2 = -241$, $x_3 = 0.78 \cdot 10^4$, and $x_4 = -2.54$

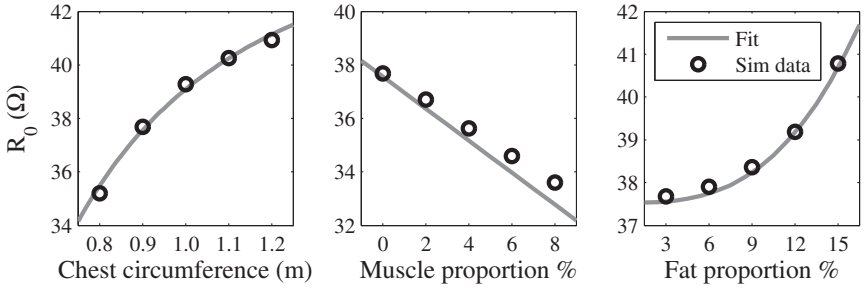

Fig. 4. Simulated impedances for variances of chest circumference, muscle proportion, and fat proportion together with the linear equation fitting holding two of the three variables fixed at: 90 cm chest circumference, 3% of fat radius proportion and/or no added muscle. Increases in impedance in response to chest circumference drops off with higher values of impedance. Increases in muscle proportion decreases the impedance linearly whereas increases in fat proportion increases the impedance in an exponential fashion in the ranges explored.

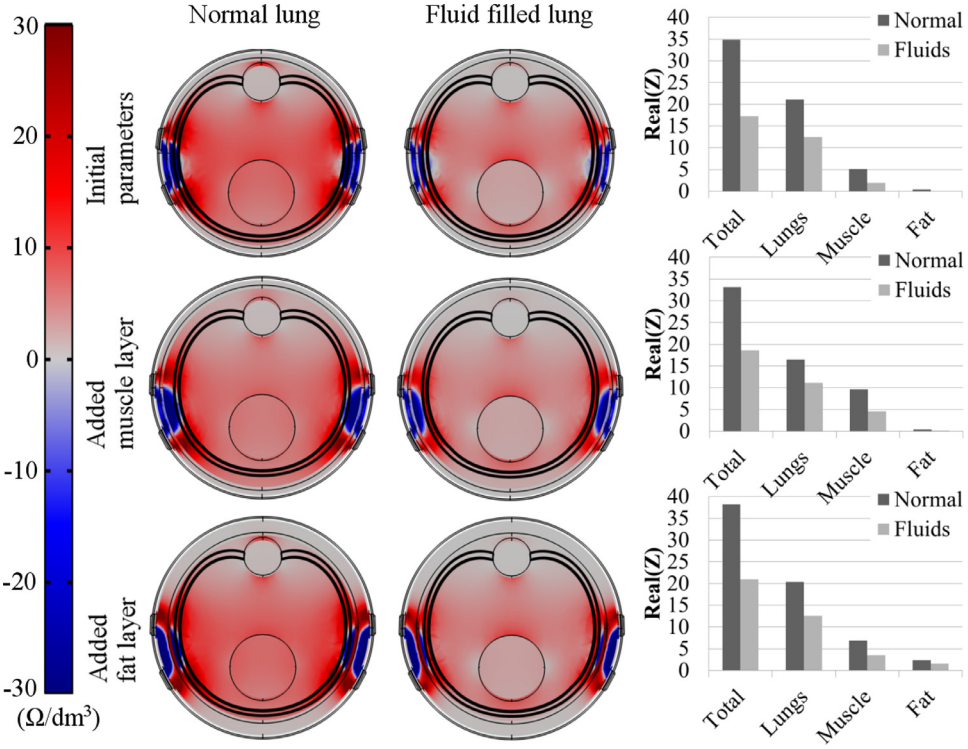

Fig. 5. Volume impedance density, the local contribution to the total transfer impedance (Ω/dm^3), for three example simulation settings ("initial parameters" (90 cm chest circumference and 1 cm of fat), increased muscle layer (added 1 cm of muscle), and increased fat layer (added 1 cm of fat)) with normal and fluid filled lungs at 10 kHz. Note that since the volume impedance density is the local contribution of the total transfer impedance measured it depends on the local direction of current and therefore it can contribute negatively. There are large changes close to the electrodes therefore to highlight contributions within the thorax coloring is clipped from −30 to 30 (Ω/dm^3). The bar graphs show the integrated impedance (Ω) from all, lung, muscle, and fat tissues, respectively. Increases in both muscle and fat lowers the effect of fluids since more current are going through the unaffected layers (decrease for the initial case is 50% compared to 44% and 45% for added muscle and fat, respectively). Muscle increase contributes to lower transfer impedance whereas fat increase contributes to higher transfer impedance.

(Eq. (9)). Although the proposed models provided a good fit to the data the physical interpretation of a linear combination of these factors should be limited as odd cases, e.g. a thorax of 100% fat, would not give sensible results.

3.2. Lung fluid dependencies, simulation

In this section we discuss the results that establishes the p_{fluids} parameter used in Eq. (4) to estimate the maximal change as a response to lung fluids. All 125 different thoracic combinations were simulated replacing the dielectric properties of the lung tissue with fluids. The proportion of impedance between a fluid filled to normal lung $p_{fluids} = R_{0\ (fluid)}/R_{0\ (dry)}$ was then calculated for each combination of fat, muscle and circumference. To predict this proportion the logit transformed linear Eq. (11) was used. Thus ensuring that the predicted proportion was between 0 and 1.

$$\mathrm{logit}(\hat{p}_{fluids}) = y_1 \cdot l_{chord} + y_2 \cdot l_{muscle} + y_3 \cdot k_{fat} + y_4 \cdot \theta + y_5 \qquad (12)$$

The fitting gave the following coefficients: $y_1 = -16.3$, $y_2 = 15.8$, $y_3 = 686$, $y_4 = -0.94$, and $y_5 = 5.84$. In this region as chord length and angle increases we get a larger difference between fluid and normal lungs i.e. both the coefficients y_1 and y_4 were negative whereas the coefficients for the other two variables were positive. This has the natural interpretation that as more lung tissue is placed between the electrodes it gets easier to detect fluid filled lungs while increased fat and muscle proportion make it more difficult.

The dependencies for individual tissues at 10 kHz are shown in Fig. 5, where the effect of added fat and muscle i.e. a lower contribution of the lung tissue to the total impedance at 10 kHz and subsequently a smaller reduction in response to fluid increase is seen. In total the lungs had the largest contribution to the total

Table 2
Model coefficients and performance measures for the fitting to TTI measurements from control subjects.

Parameter	Estimate	SE	t-stat	p-value
Model 1				
x_1	295	103	2.85	0.007
x_2	−5.1	1.77	−2.90	0.007
x_3	$2.72 \cdot 10^6$	$1.06 \cdot 10^6$	2.55	0.015
x_4	−25.7	18	−1.43	0.162
Model 2				
x_1	22.5	47.2	0.48	0.636
x_3	$2.85 \cdot 10^6$	$1.17 \cdot 10^6$	2.43	0.021
x_4	17.4	11.2	1.55	0.131
Model 3				
x_{chest}	8.94	8.11	1.10	0.278
$x_{fat\%}$	0.19	0.096	1.96	0.058
x_{offset}	11.9	8.15	1.46	0.153
Performance	RMSE (Ω)	MAE (%)	F-stat	r
Model 1	2.80	8.9	5.23	0.57
Model 2	3.14	10.3	2.98	0.39
Model 3	3.23	10.7	1.93	0.32
Repeat meas.	1.87	5.9	–	0.86

impedance at 10 kHz and fluid filled lungs resulted in large reductions in simulated impedance.

4. Measurement results

4.1. Model fitting to control subjects

Eq. (11) was unsuitable to fit to the measurement data from control subjects since the calculated variables θ and l_{chord} were colinear thus the slightly simpler Eq. (9) was used instead. Fitted coefficients for this eq. (Model 1), the same model omitting the muscle variable (Model 2), and a simplified linear model based solely on the chest circumference (in meters) and fatmass percentage (Model 3) are shown together with its associated statistical parameters and the simulation estimates in Table 2. The RMSE of model 1 (all calculated variables) was 2.80 Ω (MAE 8.93%) with a Pearson's r-value of 0.57. Using the measurements following breakfast to estimate errors of repeated measurements the system had a RMSE of 1.87 Ω (25 of the 36 subjects had analyzable second measurements). It should be noted that on average the impedance decreased following breakfast (−0.51 Ω) which added a bias and subsequently a slight overestimation of errors due to repeat measurements.

Both chest circumference and fat mass had coefficients with higher weights than the simulations, as can be seen in Table 2. Fat especially influenced the measure more than in the simulation. This could be due to the fact that apart from surrounding fat layer high levels of fat are associated with infiltrated fat surrounding the heart, muscles, liver, and other vital organs which was omitted from the simulation. Qualitatively the results of the simulations and the real measurements agree.

4.2. Impedance values compared to modeled values at discharge

The developed Model 1 (Table 2) was applied to the measured morphology of the HF patients and compared to the measured TTI at discharge i.e. after any overt congestion had been treated and the patient deemed stable enough to be sent home (mean HFSS at discharge 0.55 ± 0.67). This data had not been used for model development and except for entering the subject-specific measures no model parameter was tuned. The estimates correlated well with the observed discharge impedances ($r = 0.73$, $p < 0.001$). However, many patients were discharged with lower values than expected, see Fig. 6, which also resulted in a higher RMSE of 6.88 Ω and MAE of 16.6%. Refitting the model to the discharged impedance values gave coefficients within the standard errors of the coefficients found for the healthy volunteers ($x_1 = 230$, $x_2 = -2.46$, $x_3 = 2.33 \cdot 10^6$, and $x_4 = -25.7$) with the exception of the muscle variable. Aging induces larger decreases in height-adjusted muscle mass than in fat free mass index [27]. The age of the HF cohort compared the control group could therefore be the reason for the smaller coefficient for the muscle variable.

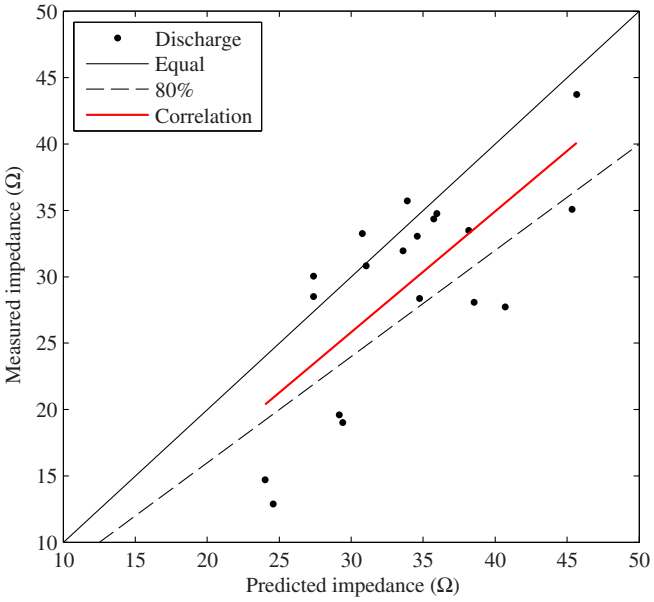

Fig. 6. Individually estimated dry impedances based on the model from control subjects applied to the discharged heart failure patients vs. the measured impedance. Correlation shown in bolded red line, points below the dashed line correspond to patients discharged below 80% of the estimated impedance. (For interpretation of the references to color in this figure legend, the reader is referred to the web version of this article.)

4.3. Fluid index during treatment

Based on Eq. (4) the fluid index was calculated from the estimated dry impedance $\hat{R}_0$ (model 1) and p_{fluids} (simulation coefficients with muscle variable set to 0). At admission the mean fluid index was 57% and all but one patient's fluid indexes were within −20–120% from admission up until discharge (Fig. 7).

Repeated measures of estimated fluid levels from patients at admission, day 1, day 2, day 3, and discharge were compared to the calculated symptom score (HFSS). The mixed-effect model found a fixed effect of 8.0% (95% CI: 5.7 – 10.3, $p < 0.001$) in the estimated fluid variable to a one point score change in the HFSS. To investigate which symptom in particular related to changes in the estimated fluid variable, the HFSS was broken into its constituent symptoms which then were explored by uni- and multivariate mixed-effects models. The uni-variate analysis found that increases in jugular venous pressure and paroxysmal nocturnal dyspnea were the symptoms which, in isolation, had the largest influence on estimated fluid difference. The same two symptoms also had the highest estimated influence in the multivariate analysis, but confidence intervals were large (Table 3). The only symptom with a p-value below 0.05 in the multivariate analysis was paroxysmal nocturnal dyspnea ($p = 0.043$) closely followed by lung crackles ($p = 0.061$). No other symptom reached a p-value below 0.1.

Table 3
Individual symptoms compared with the estimated fluid index percentage for patients treated for acute heart failure. Fixed effect estimates were derived in both a univariate and multivariate linear mixed effect analysis with patient specific intercepts as random effects. Abbreviations: PND, paroxysmal nocturnal dyspnea; red., reduced; tol., tolerance; JVP, jugular venous pressure.

Symptom	Univariate			Multivariate		
	Estimate	95% CI	p-value	Estimate	95% CI	p-value
Major						
PND	31.3	(20.0 – 42.6)	<0.001	14.1	(0.5 – 27.7)	0.043
Basal crackles	22.1	(13.4 – 30.9)	<0.001	10.4	(−0.5 – 21.2)	0.061
Hepatojugular reflex	24.7	(14.1 – 35.3)	<0.001	7.2	(−5.8 – 20.2)	0.274
Third heart sound	7.1	(−9.9 – 24.0)	0.410	−2.7	(−17.2 – 11.9)	0.718
Minor						
Orthopnea	21.6	(12.0 – 31.2)	<0.001	5.1	(−4.9 – 15.2)	0.311
Red. exercise tol.	8.3	(-3.3 – 19.8)	0.159	−0.7	(−10.2 – 8.7)	0.875
Tachycardia	21.4	(5.9 – 36.9)	0.007	2.6	(−12.0 – 17.2)	0.724
Increased JVP	31.5	(18.3 – 44.8)	<0.001	13.5	(−3.3 – 30.2)	0.113
Hepatomegaly	16.0	(2.6 – 29.5)	0.020	−10.6	(−23.4 – 2.3)	0.105
Peripheral edema	26.3	(13.3 – 39.3)	<0.001	6.0	(-8.0 – 20.0)	0.396

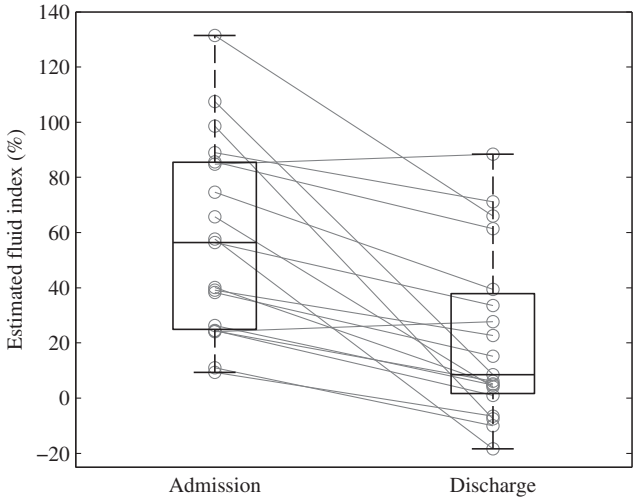

Fig. 7. Boxplots showing the median, the range, and the 25th and 75th percentile of thoracic fluid index at admission for acutely decompensated HF and discharge. Individual patient trajectories are shown as gray circles connected with lines.

4.4. Comparison with an index ratio of extracellular fluids

Other methods to establish fluid indices from bio-impedance have been suggested [28–30]. In Sakaguchi et al. [28] and Skrabal et al. [30] ratios of extracellular fluids (ECF) were used. The ratio of ECF to body water is easier to establish since it implicitly assumes tissue homogeneity and therefore does not need any anthropometric measures. We compared the segmental thoracic ECF ratio to our proposed metric in explaining the heart failure severity score using the Akaike information criterion (AIC) [31]. The ECF ratio had an AIC of 339.47 which was inferior to the fluid index with an AIC of 327.55. This large difference in AIC (12) translates to a probability of minimizing information loss with the ECF ratio of less than 0.3% as compared to the fluid index. Nevertheless, both metrics follow changes in surrogate markers of fluids during treatment (fluid index $r = 0.82$ and $r = -0.89$, ECF ratio $r = 0.86$ and $r = -0.73$ for bodyweight change and R0 change respectively, figure in appendix). However, in our sample the spread of ECF ratio at admission was very large and covered the discharge measures (admission ECF ratio: $44.9 \pm 7.4 (23.6 - 54.9)$ discharge ECF ratio: $38.8 \pm 5.4 (27.8 - 47.7)$) an issue not seen with the fluid index. The ECF ratio might therefore be less suited to establish guide values.

5. Discussion

Tracking changes in bioimpedance levels for HF patients have been employed successfully to measure fluid changes [18,32–34] and risk of hospitalization [35,36]. However, at admission or when periods of worsening are detected these trends give no guidance on when the period of risk has been adequately resolved.

A personalized fluid index obtained by normalizing impedance measures would add to the impedance concept by providing a target of a dry state. This could be inferred from periods of established euvolemia but in absence of which, morphological parameters could be used to infer a normal impedance value. In this paper we present a normalization method for bioimpedance measured across the chest. The simulations show that the largest contribution of the total impedance between 10 kHz and 1 MHz comes from the lungs, but tissue variation close to the electrodes have a large contribution in proportion to their volume. Variations of both subcutaneous fat and thoracic muscle influences the current paths and thus disproportionally affect the resulting measured value.

The simulations tended to produce higher impedance values when compared to actual recordings. Overestimation of impedance levels has also been reported with 3D reconstructed models in this frequency range when using Gabriels estimates [17]. Anisotropy in dielectric properties and the fact that Gabriels estimates in the domain <1 MHz are associated with considerable uncertainty [37] could be reasons for this. For example, Sanchez et al. report 2-fold higher conductivities during in-vivo measurements of human lung tissue compared to Gabriels estimates [38]. Qualitatively the simulation estimates and the estimates from actual measurements agree. The simulations also informed the modeling of the investigated components and resulted in models with a better fit than a simple linear combination of the factors. In this way, the simulation model provided a useful tool for modeling the impact of chest geometry and composition as captured by simple anthropometric measurements on the recorded impedance value.

For the HF patients the estimated impedances correlated with their discharge impedance although many of the patients were discharged below 80% of the model expected value. It is possible that the model which was fitted to younger healthy volunteers was not well suited for the more elderly population, especially the link between fat free mass index and thoracic muscle is different in this cohort [27]. However, refitting the model to the discharge values of the HF patients induced only modest effects on coefficient estimates, with the largest deviations for the FFMi coefficient. A

possible interpretation of this finding is that the model produces reasonable estimates but that the variance in discharged HF patients is high. Conductivities for some HF patients might be lower even in their asymptomatic state than for healthier patients due to chronic congestion and related tissue changes in response to this [39]. Miller et al. [40] reported a 30% mean increase in blood volume, with substantial variance, for a cohort of HF patients discharged after an episode of acute decompensation compared to estimated normal levels. Other supporting evidence of higher conductivities in sicker patients are findings that NYHA class[2] [29], NT-proBNP levels [18,41] and mortality [42] are associated with reduced impedance. Anecdotally, the two patients discharged with the largest estimated fluid indices in our cohort had a very poor prognosis.

As the patients symptoms improved, captured by the HFSS, so did the fluid index with an estimated fixed effect of 8% for each point in symptom score improvement. Not all symptoms improved the impedance equally and the multi-variate analysis indicated that changes were likely driven by symptoms relating to lung fluids (lung crackles and paroxysmal nocturnal dyspnea). Interestingly, a finding of increased jugular venous pressure had a large estimated change on fluid index in both the uni- and multivariate analysis. Mechanisms that could explain this could be left sided congestion propagating through the pulmonary circulation, increased back pressures for lymphatic drainage of the lung and/or fluid build up in surrounding tissues (e.g. the liver) affecting the measurement; although the data is inconclusive. Symptom assessment is inherently subjective and with the small cohort these findings are tentative but in agreement with the general hypothesis that the index primarily follows pulmonary fluid build up.

In the setting of remote monitoring a target would help those remotely observing the patients to better understand the fluid status and titrate treatment. Targets of pulmonary pressures have been shown to provide effective remote monitoring with reduced hospitalizations and mortality [43]. Impedance correlates well with pulmonary pressures [44] and fluids [34]. However, two large trials testing alerts for falling intra-thoracic impedance levels, without a target, have not showed any clear benefit [45,46]. Extending remote monitoring of impedance with a target or guide value as well as a trend value might aid clinicians and/or patients when assessing the alerts. Furthermore, keeping patients within a healthy zone [47] is conceptually attractive and normalized lung impedance may play a role in this.

The presented model is a step towards this for a wearable textrode TTI measurement system with the use of simple measures that can be extracted quickly (chest-circumference and skin caliper measurements). However, the method still provides substantial variability in estimates for discharged patients and therefore it could only be used as a guide value and not as a strict threshold. Chronic congestion might lead to pulmonary tissue changes in some patients, which would alter the conductivity, and thus the patient might not be able to reach expected values, even with proper therapy. Further research looking into other characteristics and combinations with trend values are warranted to improve upon this. Another avenue to improve the model estimates would be to extract better morphology variables, e.g. directly from thoracic scans, together with a development cohort showing a broader morphology variance. For the fluid index estimations an objective comparator would help to further develop the method along with better simulation parameters and morphology. More detailed simulations could also aid in parameter extraction. For the presented simulation approach, R_0 provided the most sensitive parameter. However, explicit modeling of congestion in the interstitium, alveolar sacs and air spaces of the lung might improve parameter extraction and fluid estimates further.

[2] A common functional classification of patients often used to track the progression of HF.

6. Conclusions

Trans-thoracic bioimpedance (TTI) measurements are affected by thoracic tissue composition and geometry, of which fat folds and fat-free mass index can account for a significant part of the TTI variance in “dry” lungs. The relationship is non-linear but can be modeled to normalize measurements of TTI which might help assessment of fluid levels for HF patients, an essential treatment target. This can be achieved with a wearable textile-electrode system which provides an attractive solution for remote monitoring systems.

Conflict of interest

ICG is a Ph.D. student employed at Philips Research. AGB, JR and RA are employed by Philips Research. PG and ABG have received departmental research support from Philips.

Acknowledgment

This work was supported by the EU Marie Curie Network iCareNet under Grant no. 264738. Medical ethical approval for the two studies were given by: Medical Ethical Committee, Maastricht University Hospital, reference: “Body composition validation study”; and Medical Ethical Committee, Hospital Universitari Germans Trias i Pujol, reference: “Bio-Impedance Monitor (BIM) vest in patients admitted with Heart Failure Trial: BIM-HeFT”. Finally, the authors would like to thank Alexandra Yvonet and Jos Gelissen for the data collection of the healthy volunteers.

Supplementary material

Supplementary material associated with this article can be found, in the online version, at 10.1016/j.medengphy.2016.03.002.

References

[1] Gheorghiade M, Filippatos G, De Luca L, Burnett J. Congestion in acute heart failure syndromes: An essential target of evaluation and treatment. Am J Med 2006;119:S3–S10. (12, Supplement 1).
[2] Drazner MH, Hellkamp AS, Leier CV, Shah MR, Miller LW, Russell SD, et al. Value of clinician assessment of hemodynamics in advanced heart failure. The ESCAPE trial. Circ Heart Fail 2008;1(3):170–7.
[3] Fein A, Grossman RF, Jones JG, Goodman PC, Murray JF. Evaluation of transthoracic electrical impedance in the diagnosis of pulmonary edema. Circulation 1979;60(5):1156–60.
[4] Arad M, Zlochiver S, Davidson T, Shovman O, Shoenfeld Y, Adunsky A, et al. Estimating pulmonary congestion in elderly patients using bio-impedance technique: Correlation with clinical examination and X-ray results. Med Eng Phys 2009;31(8):959–63.
[5] Larsen FF, Mogensen L, Tedner B. Transthoracic electrical impedance at 1 and 100 kHz - a means for separating thoracic fluid compartments? Clin Physiol 1987;7(2):105–13.
[6] Seoane F, Abtahi S, Abtahi F, Ellegrd L, Johannsson G, Bosaeus I, et al. Mean expected error in prediction of total body water: A true accuracy comparison between bioimpedance spectroscopy and single frequency regression equations. Biomed Res Int 2015;2015:656323.
[7] Cole KS, Cole RH. Dispersion and absorption in dielectrics I. Alternating current characteristics. J Chem Phys 1941;9(4):341–51.
[8] Martinsen OG, Grimnes S. Bioimpedance and bioelectricity basics. Academic Press; 2011.
[9] Zlochiver S, Arad M, Radai M, Barak-Shinar D, Krief H, Engelman T, et al. A portable bio-impedance system for monitoring lung resistivity. Med Eng Phys 2007;29(1):93–100.
[10] Amir O, Rappaport D, Zafrir B, Abraham WT. A novel approach to monitoring pulmonary congestion in heart failure: Initial animal and clinical experiences using remote dielectric sensing technology. Congest Heart Fail 2013;19(3):149–55.
[11] Celik N, Gagarin R, Huang GC, Iskander M, Berg B. Microwave stethoscope: Development and benchmarking of a vital signs sensor using computer-c phantoms and human studies. IEEE Trans Biomed Eng 2014;61(8):2341–9.

[12] Reiter H, Muehlsteff J, Sipila A. Medical application and clinical validation for reliable and trustworthy physiological monitoring using functional textiles: Experience from the HeartCycle and MyHeart project. In: Proceedings of the 2011 annual international conference of the IEEE engineering in medicine and biology society,EMBC, IEEE; 2011. p. 3270–3.
[13] Ulbrich M, Muehlsteff J, Walter M, Leonhardt S. Simulation of lung edema in impedance cardiography. In: Proceedings of the computing in cardiology (CinC); 2012. p. 33–6.
[14] Beckmann L, van Riesen D, Leonhardt S. Optimal electrode placement and frequency range selection for the detection of lung water using Bioimpedance Spectroscopy. In: Proceedings of the twenty ninth annual international conference of the IEEE engineering in medicine and biology society, EMBS 2007; 2007. p. 2685–8.
[15] Yang F, Patterson RP. A simulation study on the effect of thoracic conductivity inhomogeneities on sensitivity distributions. Ann Biomed Eng 2008;36(5):762–8.
[16] Gabriel S, Lau RW, Gabriel C. The dielectric properties of biological tissues: II. Measurements in the frequency range 10 Hz to 20 GHz. Phys Med Biol 1996;41(11):2251.
[17] Pettersen FJ, Høgetveit JO. From 3d tissue data to impedance using Simpleware ScanFE+IP and COMSOL Multiphysics a tutorial. J Electr Bioimpedance 2011;2(1):13–32.
[18] Cuba-Gyllensten I, Gastelurrutia P, Riistama J, Aarts R, Nuñes J, Lupon J, et al. A novel wearable vest for tracking pulmonary congestion in acutely decompensated heart failure. Int J Cardiol 2014;177(1):199–201.
[19] Ho KK, Pinsky JL, Kannel WB, Levy D, Pitt B. The epidemiology of heart failure: The Framingham study. J Am Coll Cardiol 1993;22(4s1):A6–A13.
[20] Pascual-Figal DA, Domingo M, Casas T, Gich I, Ordoez-Llanos J, Martnez P, et al. Usefulness of clinical and NT-proBNP monitoring for prognostic guidance in destabilized heart failure outpatients. Eur Heart J 2008;29(8):1011–18.
[21] Troughton RW, Frampton CM, Yandle TG, Espine EA, Nicholls MG, Richards AM. Treatment of heart failure guided by plasma aminoterminal brain natriuretic peptide (N-BNP) concentrations. Lancet 2000;355(9210):1126–30.
[22] Buendia R, Seoane F, Bosaeus I, Gil-Pita R, Johannsson G, Ellegård L, et al. Robustness study of the different immittance spectra and frequency ranges in bioimpedance spectroscopy analysis for assessment of total body composition. Physiol Meas 2014;35(7):1373.
[23] VanItallie TB, Yang MU, Heymsfield SB, Funk RC, Boileau RA. Height-normalized indices of the body's fat-free mass and fat mass: potentially useful indicators of nutritional status.. Am J Clin Nutr 1990;52(6):953–9.
[24] Kyle UG, Schutz Y, Dupertuis YM, Pichard C. Body composition interpretation: Contributions of the fat-free mass index and the body fat mass index. Nutrition 2003;19(7-8):597–604.
[25] Heymsfield SB, Gallagher D, Mayer L, Beetsch J, Pietrobelli A. Scaling of human body composition to stature: new insights into body mass index. Am J Clin Nutr 2007;86(1):82–91.
[26] Durnin JVGA, Womersley J. Body fat assessed from total body density and its estimation from skinfold thickness: measurements on 481 men and women aged from 16 to 72 Years. Br J Nutr 1974;32(01):77–97.
[27] Kyle UG, Genton L, Hans D, Karsegard L, Slosman DO, Pichard C. Age-related differences in fat-free mass, skeletal muscle, body cell mass and fat mass between 18 and 94 years. Eur J Clin Nutr 2001;55(8):663–72.
[28] Sakaguchi T, Yasumura K, Nishida H, Inoue H, Furukawa T, Shinouchi K, et al. Quantitative assessment of fluid accumulation using bioelectrical impedance analysis inpatients with acute decompensated heart failure. Circ J 2015;79(12):2616–22.
[29] Shochat M, Shotan A, Blondheim DS, Kazatsker M, Dahan I, Asif A, et al. Derivation of baseline lung impedance in chronic heart failure patients: use for monitoring pulmonary congestion and predicting admissions for decompensation. J Clin MonitComput 2014;29(3):341–9 Pubmed ID: 25193676.
[30] Skrabal F, Pichler GP, Gratze G, Holler A. Adding hemodynamic and fluid leads to the ECG. Part I: The electrical estimation of BNP, chronic heart failure (CHF) and extracellular fluid (ECF) accumulation. Med Eng Phys 2014;36(7):896–904.
[31] Akaike H. A new look at the statistical model identification. IEEE Trans Autom Control 1974;19(6):716–23.
[32] Dovancescu S, Torabi A, Mabote T, Caffarel J, Kelkboom E, Aarts R, et al. Sensitivity of a wearable bioimpedance monitor to changes in the thoracic fluid content of heart failure patients. In: Computing in Cardiology Conference (CinC), 2013; 2013. p. 927–30.
[33] Yu CM, Wang L, Chau E, Chan RHW, Kong SL, Tang MO, et al. Intrathoracic impedance monitoring in patients with heart failure. Circulation 2005;112(6):841–8.
[34] Becher J, Kaufmann SG, Paule S, Fahn B, Skerl O, Bauer WR, et al. Device-based impedance measurement is a useful and accurate tool for direct assessment of intrathoracic fluid accumulation in heart failure. Europace 2010;12(5):731–40.
[35] Cuba Gyllensten I, Bonomi AG, Goode KM, Reiter H, Habetha J, Amft O, Cleland JG. Early Indication of Decompensated Heart Failure in Patients on Home-Telemonitoring: A Comparison of Prediction Algorithms Based on Daily Weight and Noninvasive Transthoracic Bio-impedance. JMIR Med Inform 2016;4(1,e3) Pubmed ID: 26892844.
[36] Sarkar S, Koehler J. A dynamic risk score to identify increased risk for heart failure decompensation. IEEE Trans Biomed Eng 2013;60(1):147–50.
[37] Gabriel C, Peyman A, Grant EH. Electrical conductivity of tissue at frequencies below 1 MHz. Phys Med Biol 2009;54(16):4863.
[38] Sanchez B, Vandersteen G, Martin I, Castillo D, Torrego A, Riu PJ, et al. In vivo electrical bioimpedance characterization of human lung tissue during the bronchoscopy procedure. A feasibility study. Med Eng Phys 2013;35(7):949–57.
[39] Kee K, Naughton MT. Heart failure and the lung. Circ J 2010;74(12):2507–16.
[40] Miller WL, Mullan BP. Understanding the heterogeneity in volume overload and fluid distribution in decompensated heart failure is key to optimal volume management role for blood volume quantitation. JACC Heart Fail 2014;2(3):298–305.
[41] Malfatto G, Corticelli A, Villani A, Giglio A, Rosa FD, Branzi G, et al. Transthoracic bioimpedance and brain natriuretic peptide assessment for prognostic stratification of outpatients with chronic systolic heart failure. Clin Cardiol 2013;36(2):103–9.
[42] Zile MR, Sharma V, Johnson JW, Warman EN, Baicu CF, Bennett TD. Prediction of all-cause mortality based on the direct measurement of intrathoracic impedance. Circ Heart Fail 2016;9(1):e002543.
[43] Abraham WT, Adamson PB, Bourge RC, Aaron MF, Costanzo MR, Stevenson LW, et al. Wireless pulmonary artery haemodynamic monitoring in chronic heart failure: a randomised controlled trial. Lancet 2011;377(9766):658–66.
[44] Malfatto G, Blengino S, Perego GB, Branzi G, Villani A, Facchini M, et al. Transthoracic impedance accurately estimates pulmonary wedge pressure in patients with decompensated chronic heart failure. Congest Heart Fail 2012;18(1):25–31.
[45] van Veldhuisen DJ, Braunschweig F, Conraads V, Ford I, Cowie MR, Jondeau G, et al. For the DOT-HF investigators, intrathoracic impedance monitoring, audible patient alerts, and outcome in patients with heart failure / clinical perspective. Circulation 2011;124(16):1719–26.
[46] Böhm M, Drexler H, Oswald H, Rybak K, Bosch B, Butter C, et al. on behalf of on Behalf of the OptiLink HF Study Investigators "Fluid status telemedicine alerts for heart failure: a randomized controlled trial". Eur Heart J 2016:ehw099.
[47] Cleland JGF, Antony R. It makes SENSE to take a safer road. Eur Heart J 2011;32(18):2225–7.
[48] Cuba-Gyllensten I, Gastelurrutia P, Riistama J, Aarts R, Nuñez J, Lupon J, Bayes–Genis A. A novel wearable vest for tracking pulmonary congestion in acutely decompensated heart failure. Int J Cardiol 2014;177(1):199–201.